

Magnetism in Twisted Bilayer WSe₂

Liangtao Peng,¹ Christophe De Beule,² Du Li,¹ Li Yang,^{1,3} E. J. Mele,² and Shaffique Adam^{1,2,4}

¹Department of Physics, Washington University in St. Louis, St. Louis, Missouri 63130, United States

²Department of Physics and Astronomy, University of Pennsylvania, Philadelphia, Pennsylvania 19104, USA

³Institute of Materials Science and Engineering, Washington University in St. Louis, St. Louis, Missouri 63130, USA

⁴Department of Materials Science and Engineering,

National University of Singapore, 9 Engineering Drive 1, Singapore 117575

(Dated: March 14, 2025)

Using a self-consistent Hartree-Fock theory, we show that the recently observed ferromagnetism in twisted bilayer WSe₂ [Nat. Commun. **16**, 1959 (2025)] can be understood as a Stoner-like instability of interaction-renormalized moiré bands. We quantitatively reproduce the observed Lifshitz transition as function of hole filling and applied electric field that marks the boundary between layer-hybridized and layer-polarized regimes. The former supports a ferromagnetic valley-polarized ground state below half-filling, developing a topological charge gap at half-filling for small twists. At larger twist angles there is a transition to a gapped triangular Néel antiferromagnet. The layer-polarized regime supports a stripe antiferromagnet below half-filling and a wing-shaped multiferroic ground state above half-filling. We map the evolution of these states as a function of filling factor, electric field, twist angle, and interaction strength. Beyond providing an understanding of recent experiments, our methodology is applicable to a broad class of moiré systems.

Moiré superlattice engineering of small rotational mismatches between atomically thin layers has opened up new avenues for studying strongly-correlated electronic phases in two-dimensional systems. In graphene-based moirés, such as magic-angle twisted bilayer graphene, electron-electron interactions in the nearly flat moiré bands near charge neutrality give rise to a rich phenomenology including correlated insulators [1], superconductivity [2], among others. More recently, there has been a lot of experimental progress on twisted transition metal dichalcogenides (TMDs), where strong spin-orbit coupling, topology, and in-situ moiré band engineering provide new pathways for realizing correlated quantum phases [3–5]. Here we focus on twisted bilayer WSe₂ (tWSe₂) where recent experiments have reported correlated magnetic states [6] and superconductivity [7, 8].

Critical observations in tWSe₂ remain unresolved within a free-particle framework. First, experiments at twist angle $\theta = 3.65^\circ$ reveal a quadratic boundary [6, 7] between the layer-hybridized and layer-polarized phases in the ν - V_z plane (i.e. $V_z \propto \nu^2$). Here $\nu = n/n_M$ is the filling of the valence moiré bands (with n_M the density per moiré cell) and V_z is the interlayer bias due to an applied electric field perpendicular to the layers. The single-particle theory predicts a linear boundary $V_z \propto \nu$ [9]. Second, reflective magnetic circular dichroism (MCD), which probes the out-of-plane magnetization, identifies a pronounced ferromagnetic state in a triangular region of the phase diagram near zero electric field and $\nu < 1$, which develops “wings” for $\nu > 1$ in finite electric fields and small magnetic fields [6]. By contrast, the single-particle theory predicts a U-shaped feature that tracks the Van Hove singularity (VHS). Third, a superconducting phase emerges at half-filling ($\nu = 1$) for small electric fields, transitioning into a correlated insulator with in-

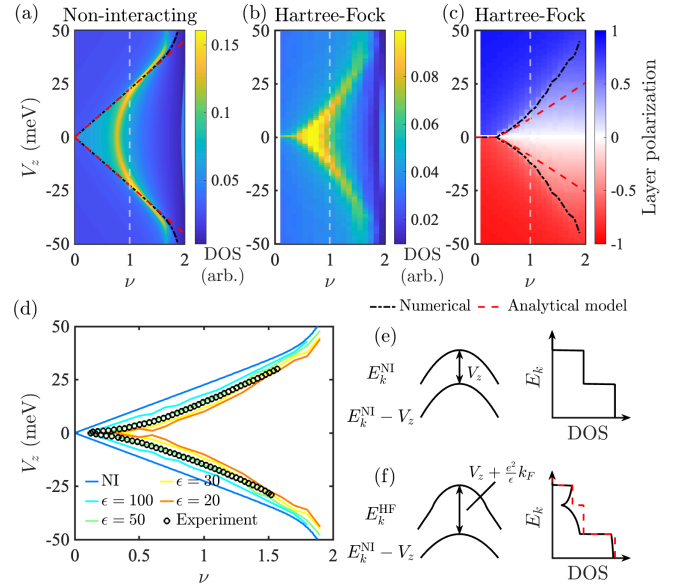


FIG. 1. Interaction-renormalized moiré bands for the *symmetry unbroken* (“parent”) Hartree-Fock state. Compared to the noninteracting theory (a), interactions shift the Van Hove singularity and soften the Lifshitz transition (b). This coincides with the change from layer-hybridized to layer-polarized regimes shown by the dotted line in (c). The red dashed line is an analytical result obtained in the absence of moiré potentials [6] we can reproduce its shape with $\theta = 3.65^\circ$ and $\epsilon \approx 30$. Panels (e) and (f) illustrate how the linear boundary in (a) follows from the constant density of states of a 2DEG while the quadratic shape arises from the interplay between Fock interactions and moiré tunneling.

creasing field strength before ultimately becoming metallic. These experimental findings motivate the need for a framework beyond the noninteracting theory.

In this Letter, we address the first two experimental observations by incorporating long-range Coulomb interactions within a Hartree-Fock (HF) scheme. The third feature, namely the observation of superconductivity at both small [7] and large [8] electric fields, has been discussed in some very recent theoretical works [10–17]. Our main results are summarized in Fig. 1. We demonstrate that both the experimentally observed phase boundary and triangular ferromagnetic region can be understood within a self-consistent mean-field theory. We interpret our findings in terms of a Stoner instability of interaction-renormalized moiré bands of the symmetry-unbroken HF state. The success of our approach suggests a more broadly applicable hierarchy of approximations, where the theory of symmetry-broken phases should be based on an unbroken parent state with strongly renormalized moiré bands. To guide future experiments, we further investigate the phase diagram as a function of hole filling and electric field, as well as the nature of the HF ground state at half-filling.

Model — Our starting point is the Hamiltonian $H = H_0 + H_{\text{int}}$ where H_0 is the noninteracting low-energy moiré theory for the valence band near valley K/K' . Due to strong Ising spin-orbit coupling, spin S_z is locked to the valley and $H_0 = \sum_{\sigma=\uparrow,\downarrow} \int d^2\mathbf{r} \psi_{\sigma}^{\dagger}(\mathbf{r}) \mathcal{H}_0^{\sigma} \psi_{\sigma}(\mathbf{r})$ with

$$\mathcal{H}_0^{\sigma} = \begin{bmatrix} \frac{\hbar^2 \nabla^2}{2m_*} + \varepsilon(\mathbf{r}) + \frac{V_z}{2} & t(-\sigma\mathbf{r}) \\ t(\sigma\mathbf{r}) & \frac{\hbar^2 \nabla^2}{2m_*} + \varepsilon(-\mathbf{r}) - \frac{V_z}{2} \end{bmatrix}, \quad (1)$$

in the layer basis within the local-stacking approximation (LSA) [18, 19]. Here we take $m_* = 0.45m_e$ for the effective mass, V_z is an interlayer bias from the applied electric field, and $\varepsilon(\mathbf{r})$ [$t(\mathbf{r})$] are intralayer [interlayer] moiré potentials. These can be written as

$$\varepsilon(\mathbf{r}) = \sum_j 2V_j \sum_{n=1}^3 \cos[\mathbf{b}_j^{(n)} \cdot \boldsymbol{\phi}(\mathbf{r}) + \psi_j], \quad (2)$$

$$t(\mathbf{r}) = \sum_j w_j \sum_{|\mathbf{K}+\mathbf{b}|=\text{const.}(j)} e^{i(\mathbf{K}+\mathbf{b}) \cdot \boldsymbol{\phi}(\mathbf{r})}, \quad (3)$$

where the first sum runs over monolayer reciprocal vectors \mathbf{b} . Here $\mathbf{b}_j^{(2,3)} = R(\pm 2\pi/3)\mathbf{b}_j^{(1)}$ and $\mathbf{K} = 4\pi\hat{x}/3a$ with $a = 3.317 \text{ \AA}$. For example, for the first star: $\mathbf{b}_1^{(1)} = 4\pi\hat{y}/\sqrt{3}a$ and $|\mathbf{K} + \mathbf{b}| = 4\pi/3a$. Here $\boldsymbol{\phi}(\mathbf{r}) = (a/a_M)\hat{z} \times \mathbf{r} + \mathbf{u}(\mathbf{r})$ is the local stacking with moiré length $a_M = a/[2\sin(\theta/2)]$ and $\mathbf{u}(\mathbf{r})$ is the displacement field due to lattice relaxation [20, 21]. The latter effectively modifies the rigid lattice moiré potentials in Eqs. (2) and (3). We find that lattice relaxation becomes significant for twist angles $\theta < 3^\circ$. In this work, we consider up to three stars of reciprocal lattice vectors in the expansion in Eqs. (2) and (3) using parameters obtained from density-functional theory (DFT) for untwisted bilayers. Computational details are in the Supplemental Material (SM) [22] and nonzero values are shown in Table I.

(V_1, ψ_1)	(V_3, ψ_3)	w_1	w_2	w_3
$(6.61, 89^\circ)$	$(0.21, -94^\circ)$	12.96	-1.95	-0.58
$\sqrt{3}$	$2\sqrt{3}$	1	2	$\sqrt{7}$

TABLE I. (top row) Parameters (in meV) of H_0 calculated from DFT for untwisted WSe₂ bilayers. (bottom row) Values for $|\mathbf{b}|$ (intralayer) and $|\mathbf{K} + \mathbf{b}|$ (interlayer) in units $4\pi/3a$.

For the twist angles we consider, the long-wavelength moiré leaves valleys decoupled, and the system has U(1) valley charge conservation, i.e., $[H, S_z] = 0$. In a single valley, the remaining symmetries are the magnetic point group $D_3(C_3) = \langle C_{3z}, C_{2y}, \mathcal{T} \rangle$ where $\mathcal{T} = i\sigma_y K$ is time reversal, and moiré translations. In addition, for $V_z = 0$ the moiré bands are spin degenerate: $E_n^{\sigma}(\mathbf{k}) \stackrel{\mathcal{P}}{=} E_n^{\sigma}(-\mathbf{k}) \stackrel{\mathcal{T}}{=} E_n^{-\sigma}(\mathbf{k})$. Here $\mathcal{P} : (\mathbf{r} \mapsto -\mathbf{r}, \tau_x)$ where τ_x flips the layers, is an ‘‘intravalley inversion’’ symmetry built into Eq. (1) by the LSA. It is only exact in the first star of the moiré potentials and is broken when either $V_z \neq 0$ (which also breaks C_{2y}) or we go beyond LSA [23]. The latter lifts the spin degeneracy of the moiré bands, which can be seen along the $\gamma - m$ line in DFT calculations [24, 25].

We treat electron-electron interactions in the self-consistent HF approximation [26] (see SM [22] for details). In particular, we consider a dual-gate screened Coulomb interaction: $V_{\mathbf{q}} = 2\pi e^2 \tanh(dq)/(\epsilon q)$ where d is the gate-to-sample distance. Throughout this work, we set $d = 20 \text{ nm}$ and treat the relative dielectric constant ϵ as a phenomenological parameter to study how physical properties depend on the interaction strength. The bandwidth of the topmost moiré band for $\theta = 3.65^\circ$ is about 40 meV [22], similar to the Coulomb energy $e^2/\epsilon a_M \approx 28 \text{ meV}$ for $\epsilon = 10$. Hence the system is in the intermediate to strongly interacting regime.

Hartree-Fock parent state — We first consider the symmetry-unbroken HF state. While this is not necessarily the ground state, it serves as a *parent state* for symmetry-broken phases. In contrast to twisted bilayer graphene [27, 28] and graphene on h-BN [29] where away from charge neutrality band-renormalization is dominated by Hartree term, we find that for tWSe₂ the self-energy is always dominated by Fock term. Hence the same exchange interactions responsible for magnetic order also dominate band renormalization. In Fig. 1 we show the density of states (DOS) of the single-particle moiré bands (a) and the parent unbroken HF state (b) for $\theta = 3.65^\circ$ as function of hole doping ν and interlayer bias V_z . We find that the DOS is significantly modified by Coulomb interactions. This reshapes the VHS and softens the Lifshitz transition between layer-hybridized and layer-polarized regimes [Fig. 1(c)] as experimentally observed [6]. In Fig. 1(d) we compare the Lifshitz transition of the parent state to the experimental data of Ref. [6]. We find that our results can reproduce the data for $\epsilon \approx 30$ where we assume that the interlayer bias is lin-

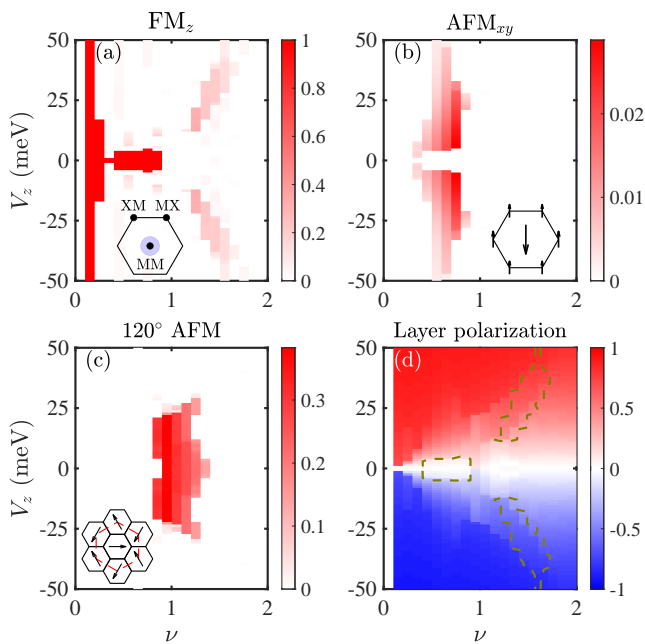


FIG. 2. Ground state magnetic order and layer polarization for $\theta = 3.65^\circ$ and $\epsilon = 25$. (a) Out-of-plane spin polarization corresponding to the FM_z phase, which exists both near charge neutrality and in regions where Fock interactions enhance the DOS [Fig. 1(b)]. The experimentally observed ferromagnetic region at small V_z below half-filling ($\nu = 1$) is clearly visible. (b) In-plane spin polarization of the IVC stripe antiferromagnet, which exists only in a small ν window in layer-polarized regions. (c) Order parameter of the 120° AFM: $\sum_{\mathbf{k}} f_{\mathbf{k}} \langle c_{\mathbf{k},\uparrow}^\dagger c_{\mathbf{k}+\mathbf{q},\downarrow} \rangle$. (d) Layer polarization where dashed lines mark the FM_z wing-shaped region from (a).

ear in the applied electric field. From the experimental geometry, one would expect $\epsilon \sim 4$; however, on very general grounds, we can anticipate a strong suppression of the Fock interactions in moiré materials that is captured phenomenologically using a larger effective dielectric constant [30]. We note that other theory works on TMDs also use larger values for the dielectric constant [31–33].

Some features of our numerical results can be understood from a toy model that neglects the moiré potentials. In this scenario, we have two parabolic bands $E_{\mathbf{k}}^{\text{NI}}$ and $E_{\mathbf{k}}^{\text{NI}} - V_z$ with $E_{\mathbf{k}}^{\text{NI}} = -k^2/2m_*$ and $V_z > 0$, as illustrated in Fig. 1(e). A Lifshitz transition occurs when the Fermi energy reaches the top of the second band, i.e., for $\nu = 2\Omega_M \int_{-V_{z,c}}^0 \text{DOS}(E) dE$, with Ω_M the moiré cell area, and the factor 2 accounts for spin. Consequently, we obtain $V_{z,c} = \pi\nu/\Omega_M m_*$ which yields the linear boundary in the single-particle limit as shown in Fig. 1(a). Adding Coulomb interactions renormalizes the top band: $E_{\mathbf{k}}^{\text{HF}} = E_{\mathbf{k}}^{\text{NI}} + \Sigma_{\mathbf{k}}^{\text{F}}$, where $\Sigma_{\mathbf{k}}^{\text{F}} = \int d^2q V_{\mathbf{k}+\mathbf{q}} f_{\mathbf{q}} / (2\pi)^2$ [34] is the Fock self-energy with $f_{\mathbf{q}}$ the occupation. The integral can be carried out analytically [22] and $E_{\mathbf{k}}^{\text{HF}} \simeq (e^2 k_{\text{F}}/\epsilon) [1 - (k/2k_{\text{F}})^2]$ where $k_{\text{F}} = \sqrt{2\pi\nu/\Omega_M}$. Hence

the Fock correction shifts the upper band upward and reduces the mass $1/m_*^{\text{F}} = 1/m_* + e^2/2\epsilon k_{\text{F}}$. For a given filling, the critical bias is now determined by

$$\nu = 2\Omega_M \left(\int_{-V_{z,c}}^{E_{\text{F}}} \frac{dEm_*}{2\pi} + \int_{E_{\text{F}}}^{e^2 k_{\text{F}}/\epsilon} \frac{dEm_*^{\text{F}}}{2\pi} \right), \quad (4)$$

where we approximated the DOS as illustrated by the red dashed line in Fig. 1(f), yielding $V_{z,c} = \pi\nu/m_* - 3e^2 k_{\text{F}}/4\epsilon$. Hence interactions lead to two effects: (i) Below filling factor $\nu_0 = 9e^2 m_*^2 / (8\pi\epsilon^2 \Omega_M)$ the Fock term shifts the top band upwards such that it accommodates all holes and the layer-hybridized regime is never reached, and (ii) the critical V_z gains a nonlinear correction given by $3e^2 k_{\text{F}}/4\epsilon \sim \sqrt{\nu}$. In Fig. 1(c), we compare these results to the full numerics using an effective $\epsilon_* = 40$. We find that this simple model captures the trend that the layer-hybridized regime is reduced. The difference is attributed to the interlayer moiré coupling, which enhances the layer-hybridized regime. Hence, we conclude that the interplay between moiré tunneling and Fock interactions give rise to the parabolic-like transition observed both in our numerics and in experiment [6]. Since these arguments are generic, we expect similar behavior in other tTMDs such as tMoTe₂ [3].

Magnetic orders — Next, we consider three symmetry-breaking magnetic orders: (i) a spin and valley polarized ferromagnetic state (FM_z) with finite S_z polarization; (ii) an intervalley coherent (IVC) antiferromagnetic state that conserves moiré translations (AFM_{xy}), and (iii) an IVC triangular Néel AFM that has a $\sqrt{3} \times \sqrt{3}$ reconstruction of the moiré cell (120° AFM). The AFM_{xy} state is an uncompensated stripe antiferromagnet while the 120° AFM hosts clockwise rotating spins for $V_z > 0$, and anticlockwise for $V_z < 0$. While all the IVC orders break \mathcal{T} and valley $U(1)$, they conserve an effective time-reversal symmetry $\mathcal{T}' = e^{i\pi\sigma_z/2}\mathcal{T}$ with $(\mathcal{T}')^2 = 1$ [35, 36].

In Fig. 2 we show the three magnetic order parameters in the ground state, for $\theta = 3.65^\circ$ as a function of filling and interlayer bias. These are S_z , $S_{x,y}$, and $\langle c_{\mathbf{k},\uparrow}^\dagger c_{\mathbf{k}+\mathbf{q},\downarrow} \rangle$ with $\mathbf{q} = \pm 4\pi\hat{y}/(3L)$. We find the FM_z phase [Fig. 2(a)] exhibits a fully-polarized phase near $V_z = 0$ below half-filling, and two “wings” with partial polarization at finite V_z . This can be understood in terms of Stoner-like ferromagnetism [37] of the HF parent state, where band renormalization from Fock interactions warps the VHS and induces a triangular region with enhanced DOS below half-filling near zero interlayer bias. These features are consistent with recent MCD measurements on tWSe₂ [6] and similar observations in tMoTe₂ [3]. We also find FM_z at small filling, which may be invisible in MCD due to the low carrier density. On the other hand, the uncompensated stripe AFM_{xy} has a small in-plane magnetization [Fig. 2(b)] and appears at finite interlayer bias below half-filling, while the 120° AFM state [Fig. 2(c)] emerges at near half-filling in a finite V_z window. More-

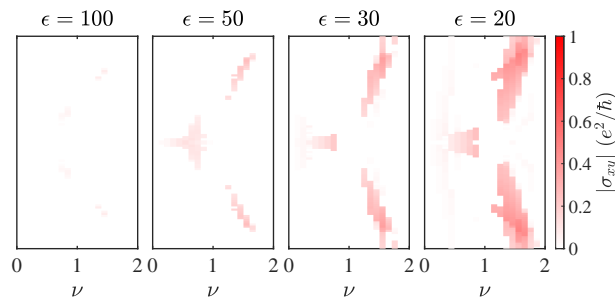


FIG. 3. Evolution of DC Hall conductivity σ_{xy} , which characterizes the degree of \mathcal{T} breaking, as a function of interlayer bias V_z and hole filling factor ν for different values of the dielectric constant ϵ . The “wing” feature emerges as a consequence of strong correlations. Contrary to $\langle S_z \rangle$, we find that σ_{xy} is a good probe for the layer-polarized FM_z phase.

over, we find this state has a finite charge gap at $\nu = 1$ as observed in experiment [6, 7]. We further show the ground-state layer polarization in Fig. 2(d). We see that below half filling the FM_z state is layer hybridized while the wings have a finite layer polarization giving rise to a multiferroic state. While the stripe AFM_{xy} is mostly layer polarized, the 120° AFM phase shows a reduced layer polarization compared to the unbroken state.

The complete ν - V_z phase diagram for $\theta = 3.65^\circ$ and $\epsilon = 25$ is shown in Fig. 4(a). Near charge neutrality, the system behaves as a 2DEG for which the Stoner mechanism gives full S_z polarization [22]. As we add holes, the FM_z phase emerges in regions of enhanced DOS of the unbroken state in accordance to the Stoner mechanism, while it gives way to a $\sqrt{3} \times \sqrt{3}$ spin density instability near half filling anticipated from the spin susceptibility [13] giving rise to the 120° AFM state. On the other hand, the IVC stripe AFM_{xy} is favored compared to the FM_z phase by the spin splitting of the dispersion which is driven by the applied field V_z [14, 38] and hence it only appears at finite interlayer bias.

DC Hall conductivity — The Hall conductivity σ_{xy} serves as an important experimental observable in transport that can probe the \mathcal{T} breaking of the FM_z phase [7]. We anticipate that σ_{xy} will soon be measured in this system both as a function of filling and interlayer bias. The Hall conductivity can be expressed as

$$\sigma_{xy} = \frac{e^2}{\hbar} \sum_n \int_{\text{MBZ}} \frac{d^2 \mathbf{q}}{(2\pi)^2} f_{n,\mathbf{q}} \Omega_{n,\mathbf{q}}, \quad (5)$$

where the sum runs over HF bands, $f_{n,\mathbf{q}}$ is the occupation and $\Omega_{n,\mathbf{q}}$ is the Berry curvature. In Fig. 3, we show σ_{xy} in the ν - V_z plane for different ϵ . The symmetry-unbroken and IVC states have vanishing σ_{xy} due to \mathcal{T}' . As a result, σ_{xy} only probes the FM_z phase. Note that while we find large $\langle S_z \rangle$ in Fig. 2(b) near charge neutrality, the Hall conductivity is absent because both the density of holes and Berry curvature is small. Moreover, for $V_z = 0$,

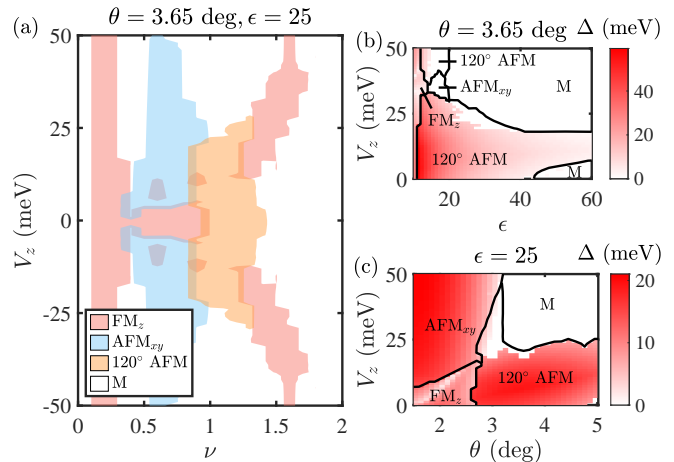


FIG. 4. Phase diagram and ground state at half filling versus twist angle and interaction strength. (a) Phase diagram for $\theta = 3.65^\circ$ and $\epsilon = 25$. The $\nu = 1$ phase diagram versus (b) interaction strength ($1/\epsilon$) and (c) twist angle, where the color gives the charge gap Δ . The gapped IVC 120° AFM persist even for weak interactions in regions where the Fermi energy is close to the VHS on the unbroken parent state (M).

regardless of the interaction strength, we find finite σ_{xy} only for $\nu < 1$, consistent with experiment [6]. Note that σ_{xy} is absent at half-filling because the gap is trivial and the 120° AFM has \mathcal{T}' symmetry. Contrary to the out-of-plane magnetization, we find that σ_{xy} is a good probe for the layer-polarized FM_z .

Correlated insulator at half-filling — At half-filling, transitions between a superconductor, a correlated insulator, and a metal were recently reported [7]. To understand the origin of these phases in WSe_2 , we examine the ground state in the self-consistent HF approximation. Our results at half-filling are shown here for completeness and are in agreement with previous reports in the literature focusing mostly on tMoTe_2 [31–33, 39, 40]. We emphasize that the filling dependence of these states has not been considered previously. In Fig. 4(b) and (c), we show the phase diagram and charge gap as a function of the interaction strength, interlayer bias, and twist angle. For small interlayer bias V_z , as we increase the interaction strength, the metallic symmetry-unbroken phase (M) gives way to a 120° AFM with a topologically trivial gap. The experimentally observed superconductivity [7, 8] is believed to be mediated by magnons of the 120° AFM. At larger V_z the single-particle bandwidth increases yielding a metallic phase except for strong interactions. However, for intermediate V_z , the 120° AFM persists even for weak interactions. This is due to the proximity of the Fermi energy to the VHS of the unbroken state. The FM_z phase only becomes the ground state for very strong interactions yielding a quantum anomalous Hall insulator with unit Chern number. For fixed $\epsilon = 25$ the FM_z state appears for small twists close to

$V_z = 0$ transitioning to a trivially gapped stripe AFM as V_z increases. For larger twists, a gapped 120° AFM dominates for small interlayer bias until $|V_z| = 25$ meV where the gap closes to a the unbroken phase due to the increased single-particle bandwidth.

Conclusions — Our self-consistent Hartree-Fock calculations offer a useful semi-quantitative guide of the ferromagnetic behavior observed experimentally. Our results emphasize the importance of first having the interaction-renormalized band structure before incorporating the effects of strong correlations. In such moiré systems, the interaction driven modification of the band structures can be significant, even at the mean-field level. As illustrated here for the case of tWSe₂, experimental observations of correlated states can be understood as a simple Stoner-like ferromagnetism once the interaction-modification of the bands are accounted for. These results highlight the importance of long-range Coulomb interactions in capturing the quantum phases in twisted 2D materials and the methods we employ are generally applicable to a wide class of moiré systems. Several future directions can be pursued within this framework. For instance, the superconducting phase at half-filling could be explored by incorporating superconducting diagrams within the Nambu formalism [41]. Additionally, the reported generalized Wigner crystals at fractional fillings [6] can be investigated by considering other translational symmetry-broken ground states.

Acknowledgments — Computation was done on Stampede3 at the Texas Advanced Computing Center through allocation PHY240263 from the ACCESS program supported by the U.S. National Science Foundation. L.P. and S.A. are supported by a start-up grant at Washington University in St. Louis. C.D.B. and E.J.M. are supported by the U.S. Department of Energy under Grant No. DE-FG02-84ER45118. D.L. and L.Y. acknowledge support from U.S. National Science Foundation DMR-2124934. We thank Valentin Crépel, Charles L. Kane, Daniel Muñoz-Segovia, and Wenjin Zhao for helpful discussions.

[1] Y. Cao, V. Fatemi, A. Demir, S. Fang, S. L. Tomarken, J. Y. Luo, J. D. Sanchez-Yamagishi, K. Watanabe, T. Taniguchi, E. Kaxiras, R. C. Ashoori, and P. Jarillo-Herrero, Correlated insulator behaviour at half-filling in magic-angle graphene superlattices, *Nature* **556**, 80 (2018).

[2] Y. Cao, V. Fatemi, S. Fang, K. Watanabe, T. Taniguchi, E. Kaxiras, and P. Jarillo-Herrero, Unconventional superconductivity in magic-angle graphene superlattices, *Nature* **556**, 43 (2018).

[3] E. Anderson, F.-R. Fan, J. Cai, W. Holtzmann, T. Taniguchi, K. Watanabe, D. Xiao, W. Yao, and X. Xu, Programming correlated magnetic states with gate-controlled moiré geometry, *Science* **381**, 325 (2023).

[4] J. Cai, E. Anderson, C. Wang, X. Zhang, X. Liu, W. Holtzmann, Y. Zhang, F. Fan, T. Taniguchi, K. Watanabe, Y. Ran, T. Cao, L. Fu, D. Xiao, W. Yao, and X. Xu, Signatures of fractional quantum anomalous Hall states in twisted MoTe₂, *Nature* **622**, 63 (2023).

[5] K. Kang, B. Shen, Y. Qiu, Y. Zeng, Z. Xia, K. Watanabe, T. Taniguchi, J. Shan, and K. F. Mak, Evidence of the fractional quantum spin Hall effect in moiré MoTe₂, *Nature* **628**, 522 (2024).

[6] P. Knüppel, J. Zhu, Y. Xia, Z. Xia, Z. Han, Y. Zeng, K. Watanabe, T. Taniguchi, J. Shan, and K. F. Mak, Correlated states controlled by a tunable van Hove singularity in moiré WSe₂ bilayers, *Nature Communications* **16**, 1959 (2025).

[7] Y. Xia, Z. Han, K. Watanabe, T. Taniguchi, J. Shan, and K. F. Mak, Superconductivity in twisted bilayer WSe₂, *Nature* **637**, 833 (2025).

[8] Y. Guo, J. Pack, J. Swann, L. Holtzman, M. Cothrine, K. Watanabe, T. Taniguchi, D. G. Mandrus, K. Barmak, J. Hone, A. J. Millis, A. Pasupathy, and C. R. Dean, Superconductivity in 5.0° twisted bilayer WSe₂, *Nature* **637**, 839 (2025).

[9] T. Devakul, V. Crépel, Y. Zhang, and L. Fu, Magic in twisted transition metal dichalcogenide bilayers, *Nature Communications* **12**, 6730 (2021).

[10] S. Kim, J. F. Mendez-Valderrama, X. Wang, and D. Chowdhury, *Theory of Correlated Insulator(s) and Superconductor at $\nu=1$ in Twisted WSe₂* (2024), [arXiv:2406.03525].

[11] J. Zhu, Y.-Z. Chou, M. Xie, and S. D. Sarma, *Theory of superconductivity in twisted transition metal dichalcogenide homobilayers* (2024), [arXiv:2406.19348].

[12] D. Guerci, D. Kaplan, J. Ingham, J. H. Pixley, and A. J. Millis, *Topological superconductivity from repulsive interactions in twisted WSe₂* (2024), [arXiv:2408.16075].

[13] C. Schrade and L. Fu, Nematic, chiral, and topological superconductivity in twisted transition metal dichalcogenides, *Physical Review B* **110**, 035143 (2024).

[14] M. Christos, P. M. Bonetti, and M. S. Scheurer, *Approximate symmetries, insulators, and superconductivity in continuum-model description of twisted WSe₂* (2024), [arXiv:2407.02393].

[15] C. Tuo, M.-R. Li, Z. Wu, W. Sun, and H. Yao, *Theory of Topological Superconductivity and Antiferromagnetic Correlated Insulators in Twisted Bilayer WSe₂* (2024), [arXiv:2409.06779].

[16] W. Qin, W.-X. Qiu, and F. Wu, *Kohn-Luttinger Mechanism of Superconductivity in Twisted Bilayer WSe₂: Gate-Tunable Unconventional Pairing Symmetry* (2024), [arXiv:2409.16114].

[17] F. Xie, L. Chen, S. Sur, Y. Fang, J. Cano, and Q. Si, *Superconductivity in twisted WSe₂ from topology-induced quantum fluctuations* (2024), [arXiv:2408.10185].

[18] J. Jung, A. Raoux, Z. Qiao, and A. H. MacDonald, Ab initio theory of moiré superlattice bands in layered two-dimensional materials, *Physical Review B* **89**, 205414 (2014).

[19] J. Jung, A. M. DaSilva, A. H. MacDonald, and S. Adam, Origin of band gaps in graphene on hexagonal boron nitride, *Nature Communications* **6**, 6308 (2015).

[20] S. Carr, D. Massatt, S. B. Torrisi, P. Cazeaux, M. Luskin, and E. Kaxiras, Relaxation and domain formation in incommensurate two-dimensional heterostructures, *Physical Review B* **98**, 224102 (2018).

- [21] M. M. A. Ezzi, G. N. Pallewela, C. De Beule, E. Mele, and S. Adam, Analytical Model for Atomic Relaxation in Twisted Moiré Materials, *Physical Review Letters* **133**, 266201 (2024).
- [22] See Supplemental Material [url] for
- [23] In this case $t^*(\mathbf{r}) \neq t(-\mathbf{r})$ and we only have $\varepsilon_2(x, y) = \varepsilon_1(-x, y)$ by $\mathcal{C}_{2y}\mathcal{T}$ symmetry. For example, \mathcal{P} symmetry is broken by $\arg(w_1/w_2) \neq 0, \pi$ and $\psi_2 \neq 0, \pi$ which is the phase of the second star that is equal for both layers.
- [24] X.-W. Zhang, C. Wang, X. Liu, Y. Fan, T. Cao, and D. Xiao, Polarization-driven band topology evolution in twisted MoTe2 and WSe2, *Nature Communications* **15**, 4223 (2024).
- [25] Y. Jia, J. Yu, J. Liu, J. Herzog-Arbeitman, Z. Qi, H. Pi, N. Regnault, H. Weng, B. A. Bernevig, and Q. Wu, Moiré fractional Chern insulators. I. First-principles calculations and continuum models of twisted bilayer MoTe2, *Physical Review B* **109**, 205121 (2024).
- [26] L. Peng, G. Vignale, and S. Adam, [Many-body perturbation theory for moiré systems](#) (2025), [arXiv:2502.06968].
- [27] M. M. A. Ezzi, L. Peng, Z. Liu, J. H. Z. Chao, G. N. Pallewela, D. Foo, and S. Adam, [A self-consistent Hartree theory for lattice-relaxed magic-angle twisted bilayer graphene](#) (2024), [arXiv:2404.17638].
- [28] C. Lewandowski, S. Nadj-Perge, and D. Chowdhury, Does filling-dependent band renormalization aid pairing in twisted bilayer graphene?, *npj Quantum Materials* **6**, 1 (2021).
- [29] D. R. Klein, U. Zondiner, A. Keren, J. Birkbeck, A. Inbar, J. Xiao, M. Sidorova, M. M. A. Ezzi, L. Peng, K. Watanabe, T. Taniguchi, S. Adam, and S. Ilani, [Imaging the Sub-Moiré Potential Landscape using an Atomic Single Electron Transistor](#) (2024), [arXiv:2410.22277].
- [30] D. Foo, L. Peng, C. De Beule, E. J. Mele, and S. Adam, Exchange Effects in Twisted Bilayer Graphene (2025), in preparation.
- [31] H. Pan, M. Xie, F. Wu, and S. Das Sarma, Topological Phases in AB-Stacked MoTe2/WSe2: Z2 Topological Insulators, Chern Insulators, and Topological Charge Density Waves, *Physical Review Letters* **129**, 056804 (2022).
- [32] W.-X. Qiu, B. Li, X.-J. Luo, and F. Wu, Interaction-Driven Topological Phase Diagram of Twisted Bilayer MoTe2, *Physical Review X* **13**, 041026 (2023).
- [33] B. Li, W.-X. Qiu, and F. Wu, Electrically tuned topology and magnetism in twisted bilayer MoTe2 at $\nu_h=1$, *Physical Review B* **109**, L041106 (2024).
- [34] For a uniform electron gas the Hartree term is canceled by the jellium background.
- [35] N. Bultinck, E. Khalaf, S. Liu, S. Chatterjee, A. Vishwanath, and M. P. Zaletel, Ground State and Hidden Symmetry of Magic-Angle Graphene at Even Integer Filling, *Physical Review X* **10**, 031034 (2020).
- [36] T. Wang, M. Wang, W. Kim, S. G. Louie, L. Fu, and M. P. Zaletel, [Topology, magnetism and charge order in twisted MoTe2 at higher integer hole fillings](#) (2023), [arXiv:2312.12531].
- [37] E. C. Stoner, Collective electron ferromagnetism, *Proceedings of the Royal Society of London. Series A. Mathematical and Physical Sciences* **165**, 372 (1997).
- [38] H. C. Po, L. Zou, A. Vishwanath, and T. Senthil, Origin of Mott Insulating Behavior and Superconductivity in Twisted Bilayer Graphene, *Physical Review X* **8**, 031089 (2018).
- [39] M. Xie, H. Pan, F. Wu, and S. Das Sarma, Nematic Excitonic Insulator in Transition Metal Dichalcogenide Moiré Heterobilayers, *Physical Review Letters* **131**, 046402 (2023).
- [40] T. Wang, T. Devakul, M. P. Zaletel, and L. Fu, [Diverse magnetic orders and quantum anomalous Hall effect in twisted bilayer MoTe2 and WSe2](#) (2024), [arXiv:2306.02501].
- [41] Y. Nambu, Quasi-Particles and Gauge Invariance in the Theory of Superconductivity, *Physical Review* **117**, 648 (1960).